

Gyrotropic birefringence via electromagnon resonance in a multiferroic of spin origin

M. Ogino,^{1,*} Y. Kaneko,² Y. Tokura,^{1,2,3} and Y. Takahashi^{1,2}¹Quantum-Phase Electronics Center (QPEC) and Department of Applied Physics, The University of Tokyo, Tokyo 113-8656, Japan²RIKEN Center for Emergent Matter Science (CEMS), Wako 351-0198, Japan³Tokyo College, The University of Tokyo, Tokyo, 113-8656, Japan

(Received 29 October 2019; accepted 26 May 2020; published 16 June 2020)

We investigate the gyrotropic birefringence (GB) that is a light-propagation-direction-dependent nonreciprocal response of birefringence, arising from the dynamical magnetoelectric coupling in a multiferroic manganite with spin-cycloid order in terms of time-domain terahertz polarimetry. The GB shows up as the enhanced nonreciprocal optical rotation on electromagnon resonance. The magnitude of the GB is found to scale with the bilinear coupling of ferroic order parameters $P \cdot M$ (P : electric polarization, M : magnetization) through the magnetic-field dependence with spin-flop transition. Quantitative spectral analysis reveals that the intermode coupling of electromagnon and antiferromagnetic resonance plays an essential role for the enhancement of the GB.

DOI: [10.1103/PhysRevResearch.2.023345](https://doi.org/10.1103/PhysRevResearch.2.023345)

I. INTRODUCTION

The existence of magnetoelectric (ME) coupling has been exemplified in certain classes of crystalline solids [1–5]. Since the additional ME coupling modifies the Maxwell's equations, novel electromagnetic phenomena have been predicted in such materials. In particular, the interaction between the electromagnetic field of light and the ME coupling gives rise to the exotic optical effects characterized by nonreciprocity [6,7]. In the ME materials, the free energy with respect to the electric (E_i) and magnetic (H_i) fields includes the coupling term $\alpha_{ij}E_iH_j$ ($i, j = x, y, z$), where α_{ij} is an element of the ME tensor α . Accordingly, the electric polarization P (or magnetization M) is induced by H (or E) as $\Delta P = \alpha H$ (or $\Delta M = \alpha E$). The diagonal ME coupling ($i = j$), i.e., $\alpha_{ii}E_iH_i$, can be realized in the multiferroics, ME monopole systems [5,8], and topological insulators, in which the ME coupling is specifically referred to as axionic term [4,9,10]. In multiferroics, the ME coupling is associated with the ferroic order parameters, i.e., P and M , enabling the control of the ME coupling by the external field. As a consequence of the light-matter interaction with the diagonal ME coupling, the emergence of unconventional optical rotation is suggested, which is referred to as gyrotropic birefringence (GB) [7]. Although the GB is the most fundamental feature in the optical response from the diagonal ME coupling, the observation of GB remains highly limited [11–14] and the role of the optical transition for the ME coupling is rarely understood. On the other hand, the off-diagonal ME coupling ($i \neq j$) causes the

nonreciprocal optical absorption, i.e., directional dichroism, as exemplified recently in many multiferroics [6,15–20].

In the matter with diagonal ME coupling, the induced polarization (ΔP^ω) and magnetization (ΔM^ω) through α_{ii} are always perpendicular to the electric ($E^\omega \perp \Delta P^\omega = \alpha H^\omega$) and magnetic ($H^\omega \perp \Delta M^\omega = \alpha E^\omega$) fields of light, respectively [Fig. 1(a)]. Accordingly, the resulting light propagating in the ME media exhibits the polarization rotation with nonreciprocity (see Appendix B), e.g., in a light-propagation-direction-dependent manner. It should be emphasized that the GB is essentially different from the conventional polarization rotation phenomena such as the Faraday effect and natural optical activity, which are the circular birefringence/dichroism arising from the breaking of time-reversal symmetry and chirality, respectively. Thus, the GB may lead to the novel control of light polarization. The strong ME coupling in multiferroics potentially exhibits the resonantly enhanced GB. In particular, the electromagnon, which is the collective spin excitations endowed with electric activity, produces the inherent dynamical ME coupling [21] as exemplified by the resonantly enhanced directional dichroism [19,20].

Since the spin cycloid always exhibits the ferroelectricity irrespective of the underlying lattice symmetry, many multiferroics have been found on the basis of this spin order [2,3,22]. The perovskite manganite $RMnO_3$ (R : rare earth) is probably the best known compound of the multiferroics in which the ferroelectricity induced by spin cycloid has been discovered. In addition, the electromagnon and their giant dynamical ME coupling have also been discovered [18,19,21]. Although the multiferroics with spin cycloids potentially show the strong GB on the resonance of the electromagnon in general, this novel optical character has not been examined. The optical effects are always relevant to the particular symmetry breaking of matter. The bilinear coupling of order parameters $P \cdot M$ is considered to be associated with the GB [Fig. 1(b)], while these symmetry characteristics remain elusive. $\text{Eu}_{0.55}\text{Y}_{0.45}\text{MnO}_3$ allows us to evaluate the

*Corresponding author: ogino@ce.t.u-tokyo.ac.jp

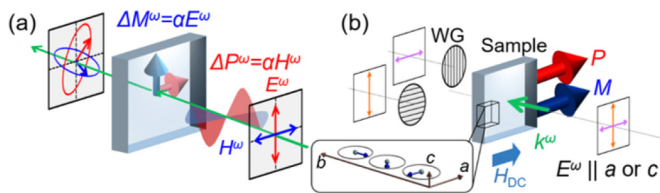


FIG. 1. (a) Schematics of gyrotropic birefringence (GB). The optical rotation arises from the diagonal ME coupling. The radiation from the magnetization (ΔM^ω) induced by the electric field (E^ω) causes the rotation of light polarization. (b) Experimental configuration for terahertz polarimetry. The incident light propagates along the b axis. Ferroelectric polarization (P) and magnetization (M) are parallel to the a axis. The optical rotation of the transmitted light is analyzed with the wire grid (WG) polarizer.

magnetization and the optical responses solely from the spin cycloid on Mn^{3+} , because Eu^{3+} and Y^{3+} are free from the magnetic moment of rare-earth ions and have no resonance in the terahertz region. In addition, $\text{Eu}_{0.55}\text{Y}_{0.45}\text{MnO}_3$ shows the spin-flop transition in the magnetic field, resulting in the flop of P [Fig. 2(a)]. Therefore, this compound enables us to track the correlation between the bilinearly coupled order parameters and GB.

In this paper, we investigated the GB in a cycloidal helimagnet $\text{Eu}_{0.55}\text{Y}_{0.45}\text{MnO}_3$ by using the time-domain terahertz polarimetry. The enhanced optical rotation was observed on the resonance of electromagnon and antiferromagnetic resonance (AFMR). The scaling behavior of GB with the bilinear coupling of ferroic order parameters $P \cdot M$ is demonstrated by tracing the GB through the magnetic-field dependence as well as by the reversal of P or M . Quantitative spectral analysis of the dynamical ME coupling reveals the essential role of

the inter-mode coupling between the electromagnon and the AFMR for the resonantly enhanced GB.

II. EXPERIMENT

A single crystal of $\text{Eu}_{0.55}\text{Y}_{0.45}\text{MnO}_3$, which has the orthorhombic $Pbnm$ lattice in the paramagnetic phase, was prepared by the floating-zone method at a feed rate of 6 mm/h in an Ar atmosphere. The ac plane samples with a thickness of $450 \mu\text{m}$ and $150 \mu\text{m}$ were used for the optical measurements below and above 5 meV, respectively. To analyze the polarization rotation induced by GB, we employed the time-domain terahertz polarimetry. For the generation of terahertz pulses, a photoconductive antenna (<5 meV) and a ZnTe (110) plane (>5 meV) were used. The terahertz light was detected by a photoconductive antenna. An external magnetic field up to 6 T was applied perpendicular to the propagating vector of light k^ω (Voigt configuration). The electric field was applied along the a axis while cooling the sample at 0 T. We performed a full polarization analysis by setting the wire grid analyzer either parallel or perpendicular, i.e., crossed Nicols geometry, to the polarization of incident light [Fig. 1(b)]. To eliminate the background for the optical rotation, we antisymmetrized the terahertz wave forms obtained in crossed Nicols geometry with respect to the sign of ferroelectric polarization ($\pm P$) as $E_{\text{CN}}(t) = [E_{\text{CN}}^{(+P)}(t) - E_{\text{CN}}^{(-P)}(t)]/2$; here, $E_{\text{CN}}^{(\pm P)}(t)$ is the temporal electric-field profile of the transmitted wave passed through the sample with $\pm P$.

III. MAGNETIC RESONANCES IN SPIN CYCLOID

A perovskite manganite $\text{Eu}_{0.55}\text{Y}_{0.45}\text{MnO}_3$ hosts the ferroelectricity induced by the spin-cycloid order. The inverse Dzyaloshinskii-Moriya mechanism describes the spin-driven electric polarization $P \propto e_{ij} \times (S_i \times S_j)$; here, $e_{i,j}$ is an unit vector connecting the neighboring spins S_i and S_j [23–25]. Figure 2(a) shows the phase diagram of $\text{Eu}_{0.55}\text{Y}_{0.45}\text{MnO}_3$ [26]. Below 22 K, the ab -plane spin cycloid with magnetic propagation vector q_m along the b axis emerges [Fig. 1(b)], giving rise to the ferroelectricity along the a axis ($P \parallel a$). The spin-cycloidal plane flops from ab to bc with increasing temperature (21 K at 0 T) or by applying the magnetic field (H_{DC}) along the a axis (4.2 T at 4 K), resulting in the flop of ferroelectric polarization from $P \parallel a$ to $P \parallel c$.

The spectra of magnetic resonances are shown in Figs. 2(b) and 2(c). The electromagnon resonance with the electric transition dipole along the a axis ($E^\omega \parallel a$) emerges in the ab - and bc -cycloid phases [0, 3.5 T for ab cycloid and 6 T for bc cycloid in Fig. 2(b)]. Two broad peaks at 2.4 meV and 8.0 meV [inset of Fig. 2(b)] have been attributed to the electromagnon driven by the exchange-striction (ES) mechanism [27,28], in which the phason mode of the spin cycloid produces the a -axis polarized electric activity irrespective of the spin plane [Fig. 2(d)]. Accordingly, the spin-flop transition at 4.2 T causes little spectral change. Figure 2(c) shows the AFMR with the magnetic transition dipole along the a axis ($H^\omega \parallel a$), in which the magnetic field of light H^ω induces the spin precession as shown in Fig. 2(e) [29]. The AFMR vanishes upon the spin-flop transition as shown in the spectra at 6 T in Fig. 2(c).

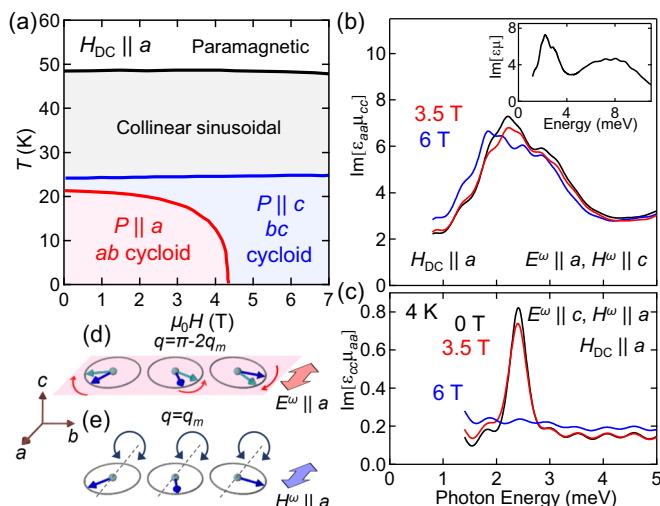


FIG. 2. (a) Magnetic phase diagram of $\text{Eu}_{0.55}\text{Y}_{0.45}\text{MnO}_3$ reproduced from Ref. [26]. (b) Spectra of the electromagnon ($\epsilon_{aa}\mu_{cc}$) in the magnetic field ($H_{\text{DC}} \parallel a$) at 4 K. Inset shows the spectra ($\epsilon_{aa}\mu_{cc}$) up to 11 meV at 4 K (0 T). (c) The spectra of antiferromagnetic resonance (AFMR) ($\epsilon_{cc}\mu_{aa}$) in the external magnetic field ($H_{\text{DC}} \parallel a$) at 4 K. Schematics of (d) electromagnon driven by the exchange-striction (ES) mechanism and (e) AFMR, respectively.

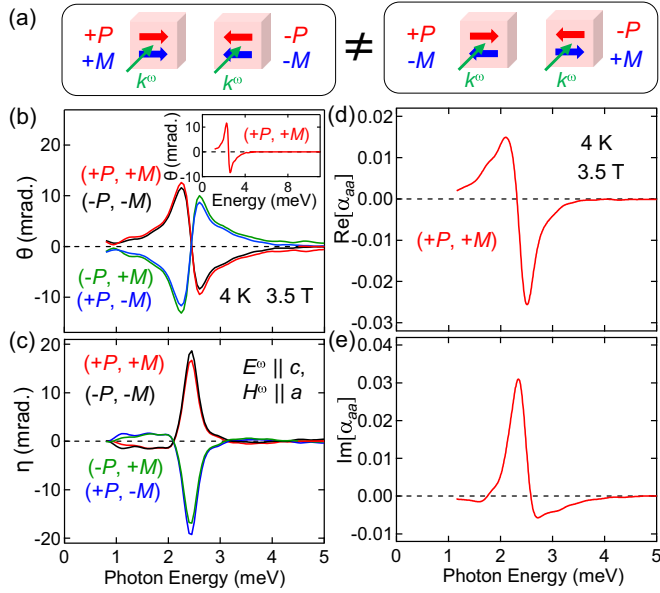


FIG. 3. (a) The optical rotation arising from the GB is characterized by the sign of $P \cdot M$. The spectra of (b) rotation angle θ and (c) ellipticity η for each ME geometry ($\pm P, \pm M$). The thickness of the sample is $450 \mu\text{m}$. The polarization of the incident light is $E^\omega \parallel c, H^\omega \parallel a$. Inset of (b) shows the spectrum of rotation angle up to 11 meV . (d) Real and (e) imaginary parts of dynamical ME spectra (α_{aa}) for $(+P, +M)$.

IV. OPTICAL ROTATION ON ELECTROMAGNON RESONANCE

To examine the GB, the optical rotation spectra, including rotation angle $\theta(\omega)$ and ellipticity $\eta(\omega)$, were measured in the ab -cycloid phase (3.5 T) with $P \parallel a$ and $M \parallel a$ [Fig. 1(b)]. [See Appendix A for the measurements of $\theta(\omega)$ and $\eta(\omega)$.] By applying magnetic field along the a axis, the magnetic point group in the spin-cycloid phase turns into $2m'm'$, which gives rise to the diagonal ME coupling $\alpha_{ii} \neq 0$ ($i = a, b, c$). As shown in Figs. 3(b) and 3(c), the clear resonance of optical rotation is observed as the dispersive structure in $\theta(\omega)$ and the peak structure in $\eta(\omega)$, while no resonance is discerned above 5 meV [inset of Fig. 3(b)]. Since the simultaneous breaking of space-inversion and time-reversal symmetries causes the GB, the rotation angle induced by the GB has odd parity with respect to P and M [Fig. 3(a)]. In fact, the observed rotation angle exhibits the sign change by the reversal of either P or M [Figs. 3(b) and 3(c)]. These results evidence that the observed optical rotation arises from the GB. Note that the possible gyrotropy induced by the magneto-optical effect, i.e., Faraday effect, is excluded in this Voigt geometry ($H_{\text{DC}} \perp k^\omega$).

To understand the role of the dynamical ME coupling for the GB, we quantitatively deduce the ME spectra as follows. The optical rotation induced by the GB can be viewed as the nonreciprocal rotation of the major axis of the refractive index ellipse [30,31]. Therefore, the off-diagonal elements of the effective dielectric tensor [$\epsilon_{ac}(\omega)$ or $\epsilon_{ca}(\omega)$], which are obtained by the terahertz polarimetry, can express the optical rotation owing to the GB. According to the Maxwell's equations with the ME coupling α_{aa} , the leading order term

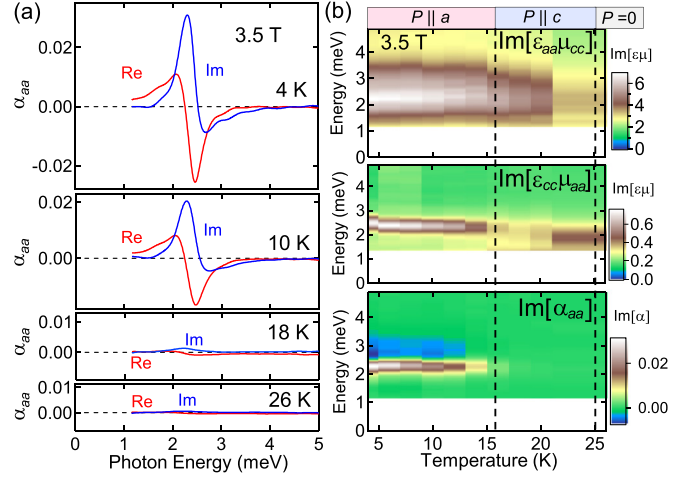


FIG. 4. (a) Temperature dependence of the complex spectra of α_{aa} at 3.5 T ($H_{\text{DC}} \parallel a$). (b) Temperature dependence of color-coded spectra of electromagnon ($\text{Im}[\epsilon_{aa}\mu_{cc}]$), AFMR ($\text{Im}[\epsilon_{cc}\mu_{aa}]$), and GB ($\text{Im}[\alpha_{aa}]$).

of ϵ_{ac} arising from α_{aa} is expressed as $\epsilon_{ac} \sim \mu_{cc} \sqrt{\frac{\epsilon_{cc}}{\mu_{aa}}} \alpha_{aa}$, where ϵ_{ii} and μ_{ii} are the dielectric and magnetic permeabilities, respectively (see Appendix C). Here we assume that $\alpha_{aa}(\omega)$ is responsible for the GB and the optical rotation out of $\alpha_{cc}(\omega)$ is negligible, because the coexistence of a -axis polarized electromagnon ($E^\omega \parallel a$) and AFMR ($H^\omega \parallel a$) should lead to the ME resonance only for $\alpha_{aa}(\omega)$ [see Figs. 2(b) and 2(c)]. The resultant spectra of $\alpha_{aa}(\omega)$ exhibit a resonance with a dispersive structure in $\text{Re}[\alpha_{aa}]$ [Fig. 3(d)] and a peak structure in $\text{Im}[\alpha_{aa}]$ [Fig. 3(e)] at 2.4 meV . It is worth noting that the nonreciprocal directional dichroism arising from the off-diagonal ME coupling α_{ca} was reported on the resonance of the electromagnon in the same material $\text{Eu}_{0.55}\text{Y}_{0.45}\text{MnO}_3$ [18]. The magnitude of the ME coupling for the directional dichroism ($\alpha_{ca} = 0.025$ at 7 T) is comparable with that of the GB in this paper ($\alpha_{aa} = 0.033$ at 3.5 T [Fig. 3(e)]).

V. CORRELATION OF GB AND SPIN CYCLOID

The correlation between the spin orders and the GB is examined for their temperature dependence [Figs. 4(a) and 4(b)]. As shown in Fig. 4(a), the resonance structure of $\alpha_{aa}(\omega)$ decreases with increasing temperature (4, 10 K) and disappears in the bc -cycloid (18 K) and the paraelectric phases (26 K). Figure 4(b) displays the temperature dependence of electromagnon ($\text{Im}[\epsilon_{aa}\mu_{cc}]$, upper panel), AFMR ($\text{Im}[\epsilon_{cc}\mu_{aa}]$, middle panel), and GB ($\text{Im}[\alpha_{aa}]$, bottom panel). The electromagnon, AFMR, and GB ($\text{Im}[\alpha_{aa}]$) have clear resonance peaks around 2.4 meV in the ab -cycloid phase. The GB disappears upon the transition from the ab ($P \parallel a$) to bc cycloid ($P \parallel c$) at 16 K, while the electromagnon and AFMR remain in the bc -cycloid phase (16–25 K). These results indicate the essential role of the ab -cycloid spin order or, equivalently, the magnetically induced P parallel to M ($P \parallel M \parallel a$) for the GB.

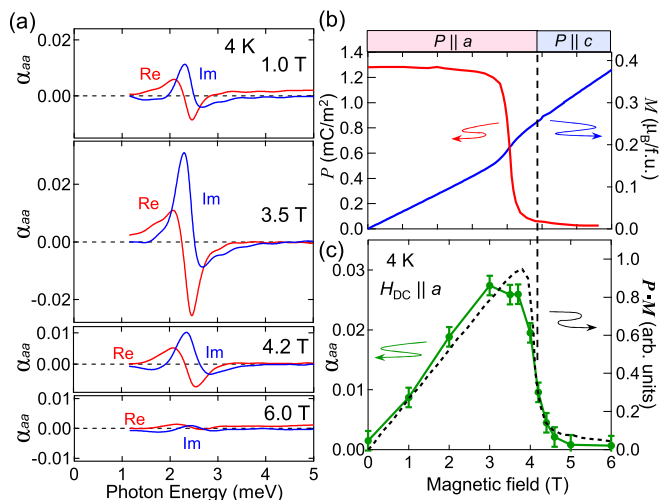


FIG. 5. (a) Magnetic field dependence of the complex spectra of α_{aa} at 4 K. (b) Magnetic field dependence of P (red line) reproduced from Ref. [26] at 2 K and M (blue line) at 4 K. M was measured with the step of 50 mT. (c) Magnetic-field dependence of peak intensity of $\text{Im}[\alpha_{aa}]$ (green line) obtained from the data in Fig. 3(c). The solid line is a guide to the eyes. The bilinearly coupled order parameters $P \cdot M$ is deduced from Fig. 3(d) (dotted black line).

VI. SCALING OF GB WITH $P \cdot M$

The magnetic-field dependence of the complex spectra of the GB [Figs. 5(a) and 5(c)] reveals the correlation between the GB and relevant order parameters (P and M). The symmetry argument suggests that the leading order of the expansion of $\alpha_{aa}(\omega)$ is proportional to $P \cdot M$ for small P and M [31]. Figure 5(b) shows the magnetic-field dependence of P and M . The P is intact below 3.5 T and the steplike suppression is observed on the spin-flop transition. The M is almost proportional to the magnetic field, while a slight anomaly is discerned at the transition point. As shown in Fig. 5(a), the magnitude of $\alpha_{aa}(\omega)$ increases with increasing magnetic field (0, 3.5 T) below the transition field (4.2 T) and rapidly decreases upon the transition to the bc -cycloid phase ($P \parallel c$, 6 T). The peak magnitude of $\text{Im}[\alpha_{aa}]$ is plotted in Fig. 5(c) (green line). The overall behavior of the GB [$\alpha_{aa}(\omega)$] along the spin-flop transition is consistent with $P \cdot M$ (dotted black line) deduced from P and M in Fig. 5(b); the linear magnetic-field dependence in the lower field and the steplike suppression on the spin-flop transition at 4.2 T. These results manifest that the bilinear coupling of ferroic order parameters $P \cdot M$ scales the magnitude of the GB. The suppression of α_{aa} is also suggested by the magnetic point group $mm'2'$ above the spin-flop transition.

VII. DISCUSSION

Hereafter, we focus on the spectral characteristics of the GB, electromagnon, and AFMR. The peak width of the GB [$\alpha_{aa}(\omega)$ in Figs. 3(d) and 3(e)] is ~ 0.4 meV, which is considerably narrower than that of electromagnon ~ 1.5 meV [Fig. 2(b)]. On the other hand, the similar spectral features including the peak position and width are discerned for AFMR [Fig. 2(c)] and GB [Fig. 3(e)]. In general, the interference

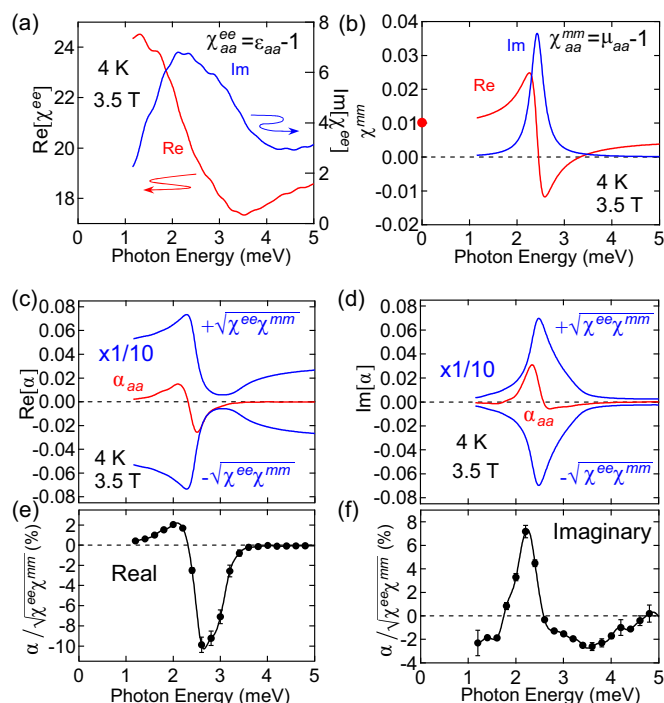


FIG. 6. (a) The complex spectra of χ_{aa}^{ee} deduced from the spectra in Fig. 2(b). (b) The complex spectra of χ_{aa}^{mm} calculated from the spectra in Fig. 2(c) with using the Lorentz function. The red point at 0 meV indicates the dc magnetic susceptibility obtained from $M - H$ curve shown in the lower panel of Fig. 3(d). (c) Real and (d) imaginary parts of the dynamical ME spectra; the observed (red line) and the upper bound of α_{aa} (blue line). The normalized ME spectra by the upper bound as $\alpha_{aa} / \sqrt{\chi_{aa}^{ee} \chi_{aa}^{mm}}$; (e) real and (f) imaginary parts deduced from the data in Figs. 4(c) and 4(d) (black lines). Error bars are plotted on the black circles at several points.

between the electric ($\langle 0 | \Delta P_a | n \rangle$) and magnetic ($\langle n | \Delta M_a | 0 \rangle$) transition dipoles is responsible for the ME resonance [32] such as

$$\alpha_{aa}(\omega) \propto \sum_n \frac{\langle 0 | \Delta P_a | n \rangle \langle n | \Delta M_a | 0 \rangle}{\omega_{n0} - \omega - i\delta}, \quad (1)$$

where the $|0\rangle$ and $|n\rangle$ denote the ground state and excited state and ω_{n0} is the angular frequency of $|n\rangle$. In the present case, the electromagnon and AFMR produce the electric and magnetic transition dipoles, respectively. The resonantly enhanced GB around 2.4 meV suggests the emergence of the intermode coupling of the magnetic excitations with different natures, i.e., the electromagnon and AFMR.

The present model material, perovskite manganite, allows the quantitative analysis of the ME spectra, leading to the understanding of the role of the magnetic excitations for the resonantly enhanced GB. The thermodynamical upper bound of the dynamical ME effect is given by the ϵ and μ as follows [33]:

$$\alpha_{aa} \leq \sqrt{\chi_{aa}^{ee} \chi_{aa}^{mm}} = \sqrt{(\epsilon_{aa} - 1)(\mu_{aa} - 1)}, \quad (2)$$

where χ_{aa}^{ee} and χ_{aa}^{mm} are the dielectric and the magnetic susceptibilities, respectively. We assumed $\epsilon_{aa} \sim \epsilon_{aa} \mu_{cc}$ [Fig. 2(b)] and $\chi_{aa}^{ee} = \epsilon_{aa} - 1$ in Fig. 6(a), because $\mu_{cc} \sim 1$ [34]. The magnetic susceptibility χ_{aa}^{mm} for the AFMR [Fig. 6(b)] is

obtained by the fitting with the Lorentz oscillator [34,35]. The high-frequency limit of χ_{aa}^{mm} is determined so as to reproduce the dc limit of $\chi_{aa}^{mm}(\omega = 0)$. In Figs. 6(c) and 6(d), the upper bounds $\sqrt{\chi_{aa}^{ee}\chi_{aa}^{mm}}$ are plotted in addition to the observed ME spectra $\alpha_{aa}(\omega)$. The coexistence of electromagnon and AFMR enhances the upper bound of α_{aa} around 2.4 meV. In contrast, the relatively small bound above 3 meV [Fig. 6(d)] is caused by the absence of the magnetic transition dipole. These results clearly indicate that the electromagnon and AFMR cooperatively give rise to the resonantly enhanced dynamical ME coupling, resulting in GB. Figures 6(e) and 6(f) show the complex ME spectra normalized by the upper bound value of $\alpha_{aa}/\sqrt{\chi_{aa}^{ee}\chi_{aa}^{mm}}$. A pronounced peak shows up at 2.4 meV, where the resonance energy of the electromagnon overlaps with that of the AFMR. The peak magnitude in the real part [Fig. 6(e)] is as large as 10% of the thermodynamical limit. Although the strong intermode coupling emerges, the bilinear coupling between electromagnon and AFMR is prohibited due to the mismatch of the wave vector of the magnons; $q = \pi - 2q_m$ for the electromagnon [28,36] and $q = q_m$ for the AFMR [29]. The higher order coupling term may produce the interference between the electromagnon and AFMR, resulting in the resonance of GB.

VIII. CONCLUSION

To summarize, we have studied GB via the electromagnon driven by ES mechanism and the AFMR in the perovskite manganite with the ab -plane spin cycloid. The emergence of GB is conclusively confirmed by the odd parity of the optical rotation with respect to P and M . The scaling behavior of GB with the bilinearly coupled ferroic order parameters such as $P \cdot M$ is demonstrated. The essential role of the intermode coupling between the electromagnon and AFMR for the GB is indicated by the spectra of dynamical ME coupling. Our results elucidate the fundamental characteristics of GB arising from the diagonal ME coupling in multiferroics and the role of the optical transition for GB in general, leading to a method for controlling polarization of light with electric field as well as magnetic field. In addition, the excitation of electromagnon resonances by the intense terahertz pulse may lead to nonlinear ME optics.

ACKNOWLEDGMENTS

This work has been supported by the JST through Grants No. JPMJPR1423 and No. JPMJCR16F1 and by JSPS KAK-ENHI (No. 17K19050 and No. 17H04845).

APPENDIX A: ROTATION ANGLE AND ELLIPTICITY SPECTRA

Figures 3(b) and 3(c) show the optical rotation spectra for the incident light polarized parallel to the c axis. The experimental geometry for the terahertz polarimetry is displayed in Fig. 7. The optical rotation caused by GB in the ac plane of $\text{Eu}_{0.55}\text{Y}_{0.45}\text{MnO}_3$ is analyzed using the wire grid polarizer in parallel and crossed Nicols geometries. The incident light is polarized parallel to the a axis [Fig. 7(a)] or to the c axis [Fig. 7(b)]. The wave forms

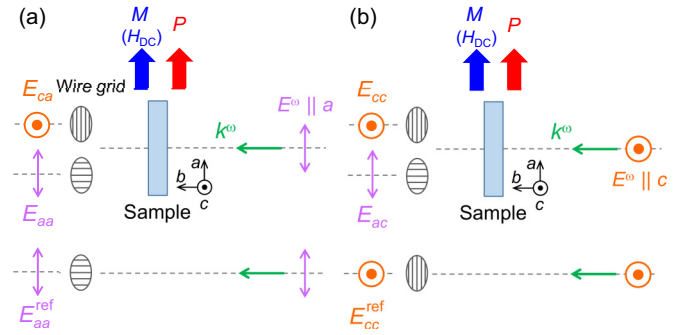


FIG. 7. Top view of experimental geometry for the terahertz polarimetry. The incident light is polarized along (a) a axis and (b) c axis. The transmitted terahertz wave form is analyzed in parallel (E_{aa} , E_{cc}) and crossed Nicols (E_{ca} , E_{ac}) geometry using the wire grid polarizer.

obtained in the crossed Nicols geometry (E_{ca} , E_{ac}) and in the parallel one (E_{aa} , E_{cc}) provide the polarization of the transmitted light. The rotation spectra in Figs. 3(b) and 3(c), including rotation angle $\theta(\omega)$ and ellipticity $\eta(\omega)$, are calculated as

$$\theta(\omega) + i\eta(\omega) \sim \frac{E_{ac}(\omega)}{E_{cc}(\omega)} = \frac{\sin \theta(\omega) + i\eta(\omega) \cos \theta(\omega)}{\cos \theta(\omega) + i\eta(\omega) \sin \theta(\omega)}. \quad (\text{A1})$$

The reference waveforms, which are used in the calculation of the effective dielectric tensor (see Appendix C), are also obtained for $E^\omega \parallel a$ [E_{aa}^{ref} in Fig. 7(a)] and $E^\omega \parallel c$ [E_{cc}^{ref} in Fig. 7(b)].

APPENDIX B: DESCRIPTION OF GYROTROPIC BIREFRINGENCE

The GB is observed as the optical rotation arising from the ME coupling in matter. We assume the diagonalized 2×2 dielectric permittivity ϵ , magnetic permeability μ , and linear ME coefficient α for the ac surface of the sample with the magnetic point group of $2m'm'$ as follows:

$$\epsilon = \begin{bmatrix} \epsilon_{xx} & 0 \\ 0 & \epsilon_{yy} \end{bmatrix}, \quad (\text{B1})$$

$$\mu = \begin{bmatrix} \mu_{xx} & 0 \\ 0 & \mu_{yy} \end{bmatrix}, \quad (\text{B2})$$

$$\alpha = \begin{bmatrix} \alpha_{xx} & 0 \\ 0 & \alpha_{yy} \end{bmatrix}. \quad (\text{B3})$$

The D and B are expressed by both the E and H ,

$$\begin{aligned} \mathbf{D} &= \epsilon_0 \epsilon \mathbf{E} + \frac{\alpha}{c} \mathbf{H} \\ \mathbf{B} &= \mu_0 \mu \mathbf{H} + \frac{\alpha}{c} \mathbf{E}, \end{aligned} \quad (\text{B4})$$

where ϵ_0 , μ_0 , and c are the dielectric permittivity, magnetic permeability, and velocity of light in vacuum, respectively. Accordingly, the Maxwell's equations are modified in the ME media. The resulting eigenpolarizations and eigenvalues are expressed by using the ϵ , μ , and α . Following Ref. [7], we introduce the effective dielectric tensor $\bar{\epsilon}$,

which can be directly measured by the time-domain terahertz polarimetry. In addition, this formalism provides the intuitive understanding of the optical rotation and the quantitative

analysis of GB. The effective dielectric tensor $\bar{\epsilon}$ has the following form:

$$\begin{bmatrix} \bar{\epsilon}_{xx} & \bar{\epsilon}_{xy} \\ \bar{\epsilon}_{yx} & \bar{\epsilon}_{yy} \end{bmatrix} = \begin{bmatrix} \epsilon_{xx}\mu_{yy} & \text{sgn}(k^\omega)\mu_{yy}\sqrt{\epsilon_{yy}\mu_{xx}}\left(\frac{\alpha_{xx}}{\mu_{xx}} - \frac{\alpha_{yy}}{\mu_{yy}}\right) \\ \text{sgn}(k^\omega)\mu_{xx}\sqrt{\epsilon_{xx}\mu_{yy}}\left(\frac{\alpha_{xx}}{\mu_{xx}} - \frac{\alpha_{yy}}{\mu_{yy}}\right) & \epsilon_{yy}\mu_{xx} \end{bmatrix}. \quad (\text{B5})$$

The higher order terms of α_{xx} and α_{yy} are omitted here. The ME terms appear in the off-diagonal elements and the sign of them depends on the sign of $E \times H$, i.e., sign of k^ω . Accordingly, the diagonal ME coupling induces the optical

rotation phenomena with nonreciprocity. With the assumption of $\alpha_{yy} = 0$ and of the fixed k^ω , the off-diagonal term $\bar{\epsilon}_{xy}$ is simplified as $\bar{\epsilon}_{xy} = \mu_{yy}\sqrt{\epsilon_{yy}\mu_{xx}}\alpha_{xx}$, which is employed in the main text.

APPENDIX C: DERIVATION OF EFFECTIVE DIELECTRIC SPECTRA FROM TIME-DOMAIN TERAHERTZ POLARIMETRY

The effective dielectric tensor, which expresses the gyrotropic optical responses, is derived from the observed electric field profiles, which include the references E_{aa}^{ref} and E_{cc}^{ref} and the transmittance signals E_{aa} , E_{ca} , E_{ac} , and E_{cc} (Fig. 7). The Fourier transformation of these electric field profiles gives these relations:

$$\frac{E_{aa}(\omega)}{E_{aa}^{\text{ref}}(\omega)} = \frac{1}{2A(\omega)} [(\Delta\epsilon(\omega) + A(\omega))T(n_+(\omega)) - (\Delta\epsilon(\omega) - A(\omega))T(n_-(\omega))], \quad (\text{C1})$$

$$\frac{E_{ca}(\omega)}{E_{aa}^{\text{ref}}(\omega)} = \frac{\bar{\epsilon}_{ca}}{2A(\omega)} [T(n_+(\omega)) - T(n_-(\omega))], \quad (\text{C2})$$

$$\frac{E_{ac}(\omega)}{E_{cc}^{\text{ref}}(\omega)} = \frac{\bar{\epsilon}_{ac}(\omega)}{2A(\omega)} [T(n_+(\omega)) - T(n_-(\omega))], \quad (\text{C3})$$

$$\frac{E_{cc}(\omega)}{E_{cc}^{\text{ref}}(\omega)} = \frac{1}{2A(\omega)} [(-\Delta\epsilon(\omega) + A(\omega))T(n_+(\omega)) - (-\Delta\epsilon(\omega) - A(\omega))T(n_-(\omega))]. \quad (\text{C4})$$

Each factor in Eqs. (C1)–(C4) is defined as follows:

$$\Delta\epsilon(\omega) = \frac{1}{2}(\bar{\epsilon}_{aa}(\omega) - \bar{\epsilon}_{cc}(\omega)), \quad (\text{C5})$$

$$A(\omega) = \sqrt{\Delta\epsilon(\omega)^2 + \bar{\epsilon}_{ac}(\omega)\bar{\epsilon}_{ca}(\omega)}, \quad (\text{C6})$$

$$T(n) = \frac{4n}{(n+1)^2} e^{i(n-1)kd}, \quad (\text{C7})$$

$$n_{\pm}(\omega) = \sqrt{\frac{1}{2}(\bar{\epsilon}_{aa}(\omega) + \bar{\epsilon}_{cc}(\omega)) \pm \sqrt{\Delta\epsilon(\omega)^2 + \bar{\epsilon}_{ac}(\omega)\bar{\epsilon}_{ca}(\omega)}}. \quad (\text{C8})$$

Solving these equations, Eqs. (C1)–(C4), the elements of the 2×2 effective dielectric tensor [left-hand side of Eq. (B5)] were obtained.

-
- [1] T. Kimura, T. Goto, H. Shintani, K. Ishizaka, T. H. Arima, and Y. Tokura, *Nature (London)* **426**, 55 (2003).
 [2] S. W. Cheong and M. Mostvov, *Nat. Mater.* **6**, 13 (2007).
 [3] F. Matsukura, Y. Tokura, and H. Ohno, *Nat. Nanotech.* **10**, 209 (2015).
 [4] X. L. Qi, T. L. Hughes, and S. C. Zhang, *Phys. Rev. B* **78**, 195424 (2008).
 [5] D. I. Khomskii, *Nat. Commun.* **5**, 4793 (2014).
 [6] Y. Tokura and N. Nagaosa, *Nat. Commun.* **9**, 3740 (2018).
 [7] R. M. Hornreich and S. Shtrikman, *Phys. Rev.* **171**, 1065 (1968).
 [8] N. A. Spaldin, M. Fechner, E. Bousquet, A. Balatsky, and L. Nordstrom, *Phys. Rev. B* **88**, 094429 (2013).
 [9] S. Zhong, J. Orenstein, and J. E. Moore, *Phys. Rev. Lett.* **115**, 117403 (2015).
 [10] F. Wilczek, *Phys. Rev. Lett.* **58**, 1799 (1987).
 [11] B. B. Krichevstov, V. V. Pavlov, R. V. Pisarev, and V. N. Gridnev, *Phys. Rev. Lett.* **76**, 4628 (1996).
 [12] A. A. Mukhin, V. D. Travkin, S. P. Lebedev, A. S. Prokhorov, and A. M. Balbashov, *J. Magn. Magn. Mater.* **183**, 157 (1998).
 [13] T. Kurumaji, Y. Takahashi, J. Fujioka, R. Masuda, H. Shishikura, S. Ishiwata, and Y. Tokura, *Phys. Rev. Lett.* **119**, 077206 (2017).
 [14] A. M. Kuzmenko, V. Dziom, A. Shuvaev, A. Pimenov, D. Szaller, A. A. Mukhin, V. Yu. Ivanov, and A. Pimenov, *Phys. Rev. B* **99**, 224417 (2019).

- [15] M. Saito, K. Taniguchi, and T. Arima, *J. Phys. Soc. Jpn.* **77**, 013705 (2008).
- [16] M. Saito, K. Ishikawa, K. Taniguchi, and T. Arima, *Phys. Rev. Lett.* **101**, 117402 (2008).
- [17] I. Kézsmárki, N. Kida, H. Murakawa, S. Bordács, Y. Onose, and Y. Tokura, *Phys. Rev. Lett.* **106**, 057403 (2011).
- [18] Y. Takahashi, R. Shimano, Y. Kaneko, H. Murakawa, and Y. Tokura, *Nat. Phys.* **8**, 121 (2012).
- [19] Y. Takahashi, Y. Yamasaki, and Y. Tokura, *Phys. Rev. Lett.* **111**, 037204 (2013).
- [20] R. Masuda, Y. Kaneko, Y. Yamasaki, Y. Tokura, and Y. Takahashi, *Phys. Rev. B* **96**, 041117(R) (2017).
- [21] A. Pimenov, A. A. Mukhin, V. Y. Ivanov, V. D. Travkin, A. M. Balbashov, and A. Loidl, *Nat. Phys.* **2**, 97 (2006).
- [22] Y. Tokura, S. Seki, and N. Nagaosa, *Rep. Prog. Phys.* **77**, 076501 (2014).
- [23] M. Kenzelmann, A. B. Harris, S. Jonas, C. Broholm, J. Schefer, S. B. Kim, C. L. Zhang, S. W. Cheong, O. P. Vajk, and J. W. Lynn, *Phys. Rev. Lett.* **95**, 087206 (2005).
- [24] H. Katsura, N. Nagaosa, and A. V. Balatsky, *Phys. Rev. Lett.* **95**, 057205 (2005).
- [25] M. Mostovoy, *Phys. Rev. Lett.* **96**, 067601 (2006).
- [26] H. Murakawa, Y. Onose, F. Kagawa, S. Ishiwata, Y. Kaneko, and Y. Tokura, *Phys. Rev. Lett.* **101**, 197207 (2008).
- [27] R. Valdés Aguilar, M. Mostovoy, A. B. Sushkov, C. L. Zhang, Y. J. Choi, S. W. Cheong, and H. D. Drew, *Phys. Rev. Lett.* **102**, 047203 (2009).
- [28] M. Mochizuki, N. Furukawa, and N. Nagaosa, *Phys. Rev. Lett.* **104**, 177206 (2010).
- [29] D. Senff, N. Aliouane, D. N. Argyriou, A. Hiess, L. P. Regnault, P. Link, K. Hradil, Y. Sidis, and M. Braden, *J. Phys.: Condens. Matter* **20**, 434212 (2008).
- [30] G. L. J. A. Rikken, C. Strohm, and P. Wyder, *Phys. Rev. Lett.* **89**, 133005 (2002).
- [31] T. Roth and G. L. J. A. Rikken, *Phys. Rev. Lett.* **85**, 4478 (2000).
- [32] S. Miyahara and N. Furukawa, *Phys. Rev. B* **89**, 195145 (2014).
- [33] W. F. Brown, R. M. Hornreich, and S. Shtrikman, *Phys. Rev.* **168**, 574 (1968).
- [34] Y. Takahashi, Y. Yamasaki, N. Kida, Y. Kaneko, T. Arima, R. Shimano, and Y. Tokura, *Phys. Rev. B* **79**, 214431 (2009).
- [35] R. Schleck, R. L. Moreira, H. Sakata, and R. P. S. M. Lobo, *Phys. Rev. B* **82**, 144309 (2010).
- [36] M. P. V. Stenberg, and R. deSousa, *Phys. Rev. B* **80**, 094419 (2009).